AGU PUBLICATIONS

Earth and Space Science

RESEARCH ARTICLE
10.1002/2014EA000045

**Key Points:**
- Annual and semiannual cycles of $CO_2$ from multiple satellites and in situ data
- Information contents of satellite $CO_2$ retrievals and vertical structures for $CO_2$
- Comparisons of ground-based and satellite $CO_2$ with models

**Correspondence to:**
X. Jiang,
xjiang7@uh.edu

**Citation:**
Jiang, X., D. Crisp, E. T. Olsen, S. S. Kulawik, C. E. Miller, T. S. Pagano, M. Liang, and Y. L. Yung (2016), $CO_2$ annual and semiannual cycles from multiple satellite retrievals and models, *Earth and Space Science*, *3*, doi:10.1002/2014EA000045.

Received 18 OCT 2014
Accepted 19 JAN 2016
Accepted article online 22 JAN 2016



# $CO_2$ annual and semiannual cycles from multiple satellite retrievals and models

**Xun Jiang[1], David Crisp[2], Edward T. Olsen[2], Susan S. Kulawik[2], Charles E. Miller[2], Thomas S. Pagano[2], Maochang Liang[3], and Yuk L. Yung[4]**

[1]Department of Earth and Atmospheric Sciences, University of Houston, Houston, Texas, USA, [2]Jet Propulsion Laboratory, California Institute of Technology, Pasadena, California, USA, [3]Research Center for Environmental Changes, Academia Sinica, Taipei, Taiwan, [4]Division of Geological and Planetary Sciences, California Institute of Technology, Pasadena, California, USA

**Abstract** Satellite $CO_2$ retrievals from the Greenhouse gases Observing SATellite (GOSAT), Atmospheric Infrared Sounder (AIRS), and Tropospheric Emission Spectrometer (TES) and in situ measurements from the National Oceanic and Atmospheric Administration - Earth System Research Laboratory (NOAA-ESRL) Surface $CO_2$ and Total Carbon Column Observing Network (TCCON) are utilized to explore the $CO_2$ variability at different altitudes. A multiple regression method is used to calculate the $CO_2$ annual cycle and semiannual cycle amplitudes from different data sets. The $CO_2$ annual cycle and semiannual cycle amplitudes for GOSAT $X_{CO2}$ and TCCON $X_{CO2}$ are consistent but smaller than those seen in the NOAA-ESRL surface data. The $CO_2$ annual and semiannual cycles are smallest in the AIRS midtropospheric $CO_2$ compared with other data sets in the Northern Hemisphere. The amplitudes for the $CO_2$ annual cycle and semiannual cycle from GOSAT, TES, and AIRS $CO_2$ are small and comparable to each other in the Southern Hemisphere. Similar regression analysis is applied to the Model for OZone And Related chemical Tracers-2 and CarbonTracker model $CO_2$. The convolved model $CO_2$ annual cycle and semiannual cycle amplitudes are similar to those from the satellite $CO_2$ retrievals, although the models tend to underestimate the $CO_2$ seasonal cycle amplitudes in the Northern Hemisphere midlatitudes and underestimate the $CO_2$ semiannual cycle amplitudes in the high latitudes. These results can be used to better understand the vertical structures for the $CO_2$ annual cycle and semiannual cycle and help identify deficiencies in the models, which are very important for the carbon budget study.

## 1. Introduction

As a result of fossil fuel emissions, atmospheric $CO_2$ demonstrates a positive trend, which varies from year to year with a range of 1.5–2 ppm from 1960 to 2014 [*Keeling et al.*, 1995; *Sarmiento and Wofsy*, 1999; *Tans and Keeling*, 2014]. Superimposed on this trend is an annual cycle resulting from the uptake and release of $CO_2$ by vegetation [*Pearman and Hyson*, 1980, 1981; *Cleveland et al.*, 1983; *Bacastow et al.*, 1985; *Keeling et al.*, 1996; *Buermann et al.*, 2007]. In addition to the trend and the annual cycle, atmospheric $CO_2$ also exhibits variability from synoptic scales to interannual timescales [*Bacastow*, 1976; *Bacastow et al.*, 1980; *Keeling and Revelle*, 1985; *Keeling et al.*, 1995; *Enting*, 1987; *Feely et al.*, 1987; *Dettinger and Ghil*, 1998; *Dargaville et al.*, 2000; *Jiang et al.*, 2010; *Keppel-Aleks et al.*, 2011; *Wang et al.*, 2011; *Jiang et al.*, 2013a].

The ground-based $CO_2$ measurement network has successfully been utilized to monitor the $CO_2$ concentrations and their trends at the surface on the hemispheric to global scale [*GLOBALVIEW-$CO_2$*, 2010]. However, the ground-based network does not have the resolution and coverage to characterize the physical processes that transport $CO_2$ throughout the atmospheric column and around the globe. Remote sensing observations from satellites provide new tools for studying the variations of atmospheric $CO_2$. Spectroscopic observations at thermal IR wavelengths are most sensitive to $CO_2$ variations in the middle troposphere [*Chahine et al.*, 2008; *Kulawik et al.*, 2010]. High-resolution spectra of reflected sunlight provide surface-weighted estimates of the column-averaged $CO_2$ dry air mole fraction [*Crisp et al.*, 2012].

Combining satellite and in situ observations and model simulations, it was found that the Madden-Julian Oscillation (MJO), Semiannual Oscillation (SAO), El Niño–Southern Oscillation (ENSO), monsoon, Northern Annular Mode (NAM), and South Atlantic Walker Circulation can influence $CO_2$ concentrations in the middle troposphere [*Li et al.*, 2010; *Jiang et al.*, 2010; *Wang et al.*, 2011; *Jiang et al.*, 2012, 2013a, 2015]. In addition to

the intraseasonal variability (e.g., MJO and SAO), ENSO, an important large-scale climate interannual variability, can influence $CO_2$ concentrations in the tropical region. During El Niño (La Niña) events, the atmospheric $CO_2$ growth rate increases (decreases) at surface stations [*Keeling et al.,* 1995; *Jones et al.,* 2001; *Nevison et al.,* 2008]. Using midtropospheric $CO_2$ data from Atmospheric Infrared Sounder (AIRS), *Jiang et al.* [2010] found that the ENSO can influence the $CO_2$ concentrations in the midtroposphere. Similar results are seen in Model for OZone And Related chemical Tracers-2 (MOZART-2) convolved midtropospheric $CO_2$, although the amplitude and spatial pattern in the model $CO_2$ are somewhat different compared to those in the AIRS midtropospheric $CO_2$ [*Jiang et al.*, 2013a]. Midtropospheric $CO_2$ can also be modulated by the strength of monsoon as a result of change in the circulation. During strong (weak) monsoon years, there are more (less) midtropospheric $CO_2$ over the Indo-Pacific Ocean compared to normal monsoon years [*Wang et al.*, 2011].

Satellite missions provide global measurements of the atmospheric $CO_2$ [*Chahine et al.*, 2008; *Kulawik et al.*, 2010; *Yokota et al.*, 2009; *Boesch et al.*, 2011; *Reuter et al.*, 2011; *Pagano et al.*, 2014]. These global and continuous $CO_2$ data offer a unique opportunity to explore the $CO_2$ variability at different altitudes. In this paper, we will investigate the annual and semiannual cycles of $CO_2$ by combining models and multiple satellite $CO_2$ retrievals from the Greenhouse gases Observing SATellite (GOSAT) [*Yokota et al.*, 2009; *Boesch et al.*, 2011; *Crisp et al.*, 2012], Atmospheric Infrared Sounder (AIRS) [*Chahine et al.*, 2008], and Tropospheric Emission Spectrometer (TES) [*Kulawik et al.*, 2010], so we can better understand the $CO_2$ annual and semiannual cycles at different altitudes and over the global domain. We will discuss data and model in section 2 and present results in section 3.

## 2. Data and Models

$CO_2$ estimates retrieved from three different satellite instruments (GOSAT, AIRS, and TES) are used in this paper. Column-averaged $CO_2$ dry air mole fraction with more weighting near the surface is retrieved from the Thermal And Near infrared Sensor for carbon Observations-Fourier Transform Spectrometer (TANSO-FTS) on GOSAT. Midtropospheric $CO_2$ estimates are retrieved from the AIRS on the NASA Aqua satellite and from the TES on the NASA Aura satellite. The above $CO_2$ data sets are compared to $CO_2$ observations from surface in situ stations from the NOAA Earth System Research Laboratory (ESRL) network and the Total Carbon Column Observing Network (TCCON). There are three types of information in these data sets. NOAA-ESRL $CO_2$ data provide $CO_2$ information at the surface. AIRS and TES $CO_2$ data provide $CO_2$ information in the midtroposphere. GOSAT and TCCON $CO_2$ data provide estimates of the $CO_2$ column-averaged dry air mole fraction. The 3-D Model for OZone And Related chemical Tracers-2, (MOZART-2) [*Horowitz et al.*, 2003; *Jiang et al.*, 2013a] and 3-D CarbonTracker [*Peters et al.*, 2007] are also used to explore the $CO_2$ annual cycle and semiannual cycle amplitudes at different pressure levels.

### 2.1. Satellite $CO_2$ Retrievals

#### 2.1.1. GOSAT $X_{CO2}$

The GOSAT TANSO-FTS collects high-resolution spectroscopic observations of reflected sunlight in the $CO_2$ bands near 1.6 and 2.06 μm and by the 0.765 μm $O_2$ A band. Its circular, 0.0157-radian diameter, instantaneous field of view yields 10.5 km diameter footprints at nadir. Over land, and over the ocean at latitudes $>20°$ from the subsolar latitude, its two-axis (along-track/cross-track) pointing mechanism obtains soundings that are separated by ~155 km (five-point mode) or ~273 km (three-point mode [*Shiomi et al.*, 2008; *Watanabe et al.*, 2008; *Kuze et al.*, 2009]). Over the ocean at latitudes $<20°$ from the subsolar latitude, the pointing mechanism targets a glint spot to provide adequate sensitivity for $X_{CO2}$ estimates. In this mode, it collects soundings at ~28 km intervals along the apparent path of the glint spot.

Column-averaged $CO_2$ dry air mole fraction ($X_{CO2}$) is retrieved from GOSAT data by the Atmospheric $CO_2$ Observations from Space (ACOS) team, using the optimal estimation approach developed for the Orbiting Carbon Observatory [*Boesch et al.*, 2006; *Connor et al.*, 2008; *O'Dell et al.*, 2012]. Data are available from http://disc.sci.gsfc.nasa.gov/acdisc/data-holdings/acos-data-holdings. GOSAT version B3.4 $X_{CO2}$ is available from June 2009 to May 2013. GOSAT B3.4 $X_{CO2}$ data used here have passed a preliminary quality filter and are recommended for the science data analysis. Comparison of $X_{CO2}$ from ACOS GOSAT and TCCON shows that they usually agree within 1–2 ppm on regional scales [*Nguyen et al.*, 2014]. We regrid the GOSAT $CO_2$ to 2° (latitude) × 2° (longitude).

**Table 1.** Summary of Time Periods and Spatial Coverage for Different $CO_2$ Data Sets

| Type | Data | Time Period | Latitude Range |
|---|---|---|---|
| Satellite $CO_2$ | GOSAT $X_{CO2}$ [*Crisp et al.*, 2012] | Jun 2009 to May 2013 | 50°S–82°N |
| | TES midtropospheric $CO_2$ [*Kulawik et al.*, 2010] | Sep 2004 to Jun 2011 | 40°S–45°N |
| | AIRS midtropospheric $CO_2$ [*Chahine et al.*, 2008] | Sep 2002 to Dec 2013 | 60°S–90°N |
| Surface $CO_2$ | NOAA ESRL $CO_2$ [*GLOBALVIEW-$CO_2$*, 2010] | Different time periods for different stations | 90°S–85°N |
| | TCCON $CO_2$ [*Washenfelder et al.*, 2006] | Different time periods for different stations | 45°S–79°N |

#### 2.1.2. AIRS Midtropospheric $CO_2$

AIRS is a cross-track scanning grating spectrometer aboard on Aqua with 2378 channels from 3.7 to 15.4 μm with a 45 km × 45 km field of view at nadir [*Aumann et al.*, 2003]. The mixing ratios of AIRS midtropospheric $CO_2$ are retrieved using the Vanishing Partial Derivative Method (VPD) [*Chahine et al.*, 2005, 2008; *Olsen and Licata*, 2015]. AIRS midtropospheric $CO_2$ retrievals are available over land and ocean and under clear and cloudy conditions. AIRS midtropospheric $CO_2$ retrievals are available at 2° (latitude) × 2.5° (longitude) from September 2002 to December 2013. The maximum sensitivity of AIRS midtropospheric $CO_2$ retrieval is from 500 hPa to 300 hPa [*Chahine et al.*, 2008]. The midtropospheric $CO_2$ retrieved via the VPD method captures the correct $CO_2$ annual cycle and trend and agrees well with the aircraft $CO_2$ from CONTRAIL [*Chahine et al.*, 2005], INTEX-NA, and SPURT with a precision ~ 1–2 ppm [*Olsen et al.*, 2008].

#### 2.1.3. TES Midtropospheric $CO_2$

TES is an imaging infrared FTS aboard on the Aura satellite, which was launched in July 2004. The TES spectral region extends from 660 $cm^{-1}$ to 2260 $cm^{-1}$ with a spectral resolution of 0.06 $cm^{-1}$ [*Beer*, 2006; *Bowman et al.*, 2006]. Midtropospheric $CO_2$ data from this instrument are available from 40°S to 45°N and from September 2004 to June 2011. Peak sensitivity of TES midtropospheric $CO_2$ data is at 511 hPa. The estimated error for TES midtropospheric $CO_2$ is ~10 ppm for a single target and ~1.3 ppm for the monthly mean average on spatial scales of 20° (latitude) × 30° (longitude) [*Kulawik et al.*, 2010]. Comparison between TES $CO_2$ with ocean surface stations from GLOBALVIEW-$CO_2$ reveals a correlation of 0.6. TES midtropospheric $CO_2$ measurements captures the correct $CO_2$ latitudinal gradient [*Kulawik et al.*, 2010]. *Kulawik et al.* [2010] compared TES midtropospheric $CO_2$ to CONTRAIL aircraft $CO_2$, AIRS midtropospheric $CO_2$, and CarbonTracker model $CO_2$ and found similar annual cycles between TES midtropospheric $CO_2$ and others. TES midtropospheric $CO_2$ also correlates well with the Carbon Tracker model $CO_2$ at the surface and 5 km [*Kulawik et al.*, 2010].

### 2.2. Surface $CO_2$ Observations

Besides the three satellite $CO_2$ data sets, we also use precise in situ $CO_2$ measurements. In situ $CO_2$ measurements include surface flask measurements from the NOAA Earth System Research Laboratory (ESRL) network [*Tans et al.*, 1998] and TCCON [*Washenfelder et al.*, 2006; *Macatangay et al.*, 2008; *Wunch et al.*, 2011]. Site information for the NOAA ESRL surface $CO_2$ is available at http://www.esrl.noaa.gov/gmd/dv/site/site_table.html. TCCON stations use a high spectral resolution FTS to record the absorption of direct sunlight by $CO_2$, $O_2$, and other gases. Under clear sky conditions, measurement precision for the TCCON column $CO_2$ is ~0.1% [*Washenfelder et al.*, 2006]. There are 20 operational sites between Ny Alesund, Norway (79°N), and Lauder, New Zealand (45°S) (http://www.tccon.caltech.edu/). Table 1 summarizes time periods and spatial coverage for all data sets.

### 2.3. Models

In this paper, two different models (MOZART-2 and CarbonTracker) are used to explore the $CO_2$ annual cycle and semiannual cycle. The MOZART-2 model is driven by the meteorological inputs every 6 h from the European Center for Medium range Weather Forecast (ECMWF)-Interim Reanalysis data from 1991 to 2012. Advection is computed every 20 min with a flux form semi-Lagrangian method [*Lin and Rood*, 1996]. The horizontal resolution of MOZART-2 is 2.8° (latitude) × 2.8° (longitude) with 45 vertical levels extending up to approximately 50 km altitude. MOZART-2 is built on the framework of the Model of Atmospheric Transport and Chemistry (MATCH). Advection, convective transport, boundary layer mixing, and wet and dry depositions are well represented in the MATCH model. Prescribed $CO_2$ sources and sinks are used as the model boundary conditions. The exchange of $CO_2$ between biosphere and atmosphere is calculated from the Carnegie-Ames Stanford Approach (CASA) biogeochemical model, which includes the effects of weather,

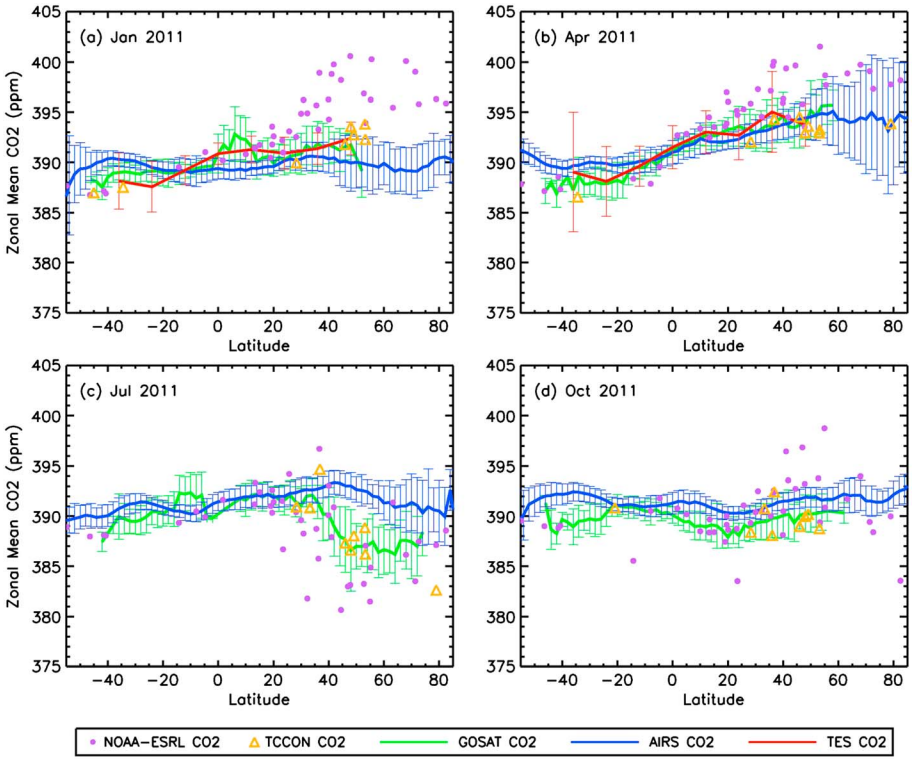


**Figure 1.** Zonal mean $CO_2$ in (a) January 2011, (b) April 2011, (c) July 2011, and (d) October 2011. Blue line is zonal mean AIRS midtropospheric $CO_2$. Red line is zonal mean TES midtropospheric $CO_2$. Green line is zonal mean GOSAT $X_{CO2}$. Error bars are the standard deviations of $CO_2$ at each latitudinal band. Purple dots are surface $CO_2$ from NOAA ESRL network. Orange triangles are TCCON $X_{CO2}$.

satellite observed Normalized Difference Vegetation Index, and fire on biosphere processes [*Olsen and Randerson*, 2004; *van der Werf et al.*, 2006; *Giglio et al.*, 2006; *Keppel-Aleks et al.*, 2012]. Air-to-sea exchange of $CO_2$ is from *Takahashi et al.* [1997]. The fire module in the model is based on Global Fire Emissions Database Version 3.1 (GFEDv3.1) [*Randerson et al.*, 2013]. Fossil fuel $CO_2$ emissions are from the Carbon Dioxide Information and Analysis Center [*Boden et al.*, 2013].

CarbonTracker 2013 has a global resolution of 3° (longitude) × 2° (latitude). Transport Model 5 (TM5) is used to represent transport in CarbonTracker. Winds used to drive TM5 are from the ECMWF operational forecast model and the ECMWF-Interim Reanalysis. Ocean uptake of $CO_2$ is taken from ocean inversions [*Jacobson et al.*, 2007] and direct measurements of seawater $pCO_2$ [*Takahashi et al.*, 2009]. The exchange between biosphere and atmosphere is from CASA biogeochemical model. The fire module in CarbonTracker is from GFEDv3.1 [*Randerson et al.*, 2013]. Fossil fuel $CO_2$ emissions are from the Miller fossil fuel emission inventory [*Miller et al.*, 2012] and ODIAC fossil fuel emission inventory [*Oda and Maksyutov*, 2011]. Surface $CO_2$ observations from NOAA-ESRL Cooperative Global Air Sampling Network and the CSIRO Air Sampling Network are assimilated in CarbonTracker. 3-D mole fractions of $CO_2$ can be downloaded from ftp://aftp.cmdl.noaa.gov/products/carbontracker/co2/.

## 3. Results

We have conducted an intercomparison for three satellite $CO_2$ data sets (GOSAT $X_{CO2}$, AIRS midtropospheric $CO_2$, and TES midtropospheric $CO_2$) with in situ $CO_2$ observations (NOAA-ESRL surface $CO_2$ and TCCON $X_{CO2}$) to check the information contents of three satellite $CO_2$ data sets in Figure 1. The averaging kernels for the GOSAT $X_{CO2}$ and TES $CO_2$ are peaked closer to the surface compared with that from AIRS midtropospheric $CO_2$. While these vertical sensitivity differences preclude the cross validation of these remote sensing data sets, they provide a unique opportunity to study the $CO_2$ variability at different altitudes on regional to global scales. Zonal mean $CO_2$ for the GOSAT $X_{CO2}$, AIRS midtropospheric $CO_2$, and TES midtropospheric

$CO_2$ in January 2011, April 2011, July 2011, and October 2011 are shown in Figure 1. Error bars in Figure 1 are the standard deviations for the zonal mean $CO_2$ at each latitudinal band. In general, the zonal average $CO_2$ for the three satellites show less variability than the NOAA-ESRL surface $CO_2$. The GOSAT and TES results are consistent with the TCCON $X_{CO2}$ data.

As shown in Figure 1a, the NOAA-ESRL surface $CO_2$ measurements and the TCCON $X_{CO2}$ data show that there is more $CO_2$ in the Northern Hemisphere (NH) than in the Southern Hemisphere (SH) in January. The latitudinal gradients of $CO_2$ are smaller in the satellite $CO_2$ (AIRS midtropospheric $CO_2$, TES midtropospheric $CO_2$, and GOSAT $X_{CO2}$) than the NOAA-ESRL surface $CO_2$. The GOSAT data extend only to ~50° latitude due to the lack of sunlight. January is the winter (summer) in the NH (SH). Release of $CO_2$ from biospheric respiration increases the atmospheric $CO_2$ concentrations near the surface in the fall and winter seasons; as a result, the atmospheric $CO_2$ concentrations are high in January in the NH. $CO_2$ uptake from vegetation in the summer removes $CO_2$ from the atmosphere and decreases the near-surface $CO_2$ concentrations in the SH in January. TCCON and GOSAT $X_{CO2}$ retrievals are sensitive to the full atmospheric column and are similar. The $CO_2$ north-south gradient in the NOAA-ESRL $CO_2$ is higher than those from the GOSAT and TCCON $X_{CO2}$, and the TES and AIRS midtropospheric $CO_2$, because the amplitude of the seasonal $CO_2$ variability decreases rapidly with altitude above the $CO_2$ surface sources/sinks. Surface $CO_2$ values are lower in the NH polar region than those at midlatitudes in January because the largest fossil fuel emissions sources are at midlatitudes [*Oda and Maksyutov*, 2011; *Boden et al.*, 2013], and $CO_2$ biospheric respiration is suppressed by the low temperature and snow/ice cover in the polar region. The midtropospheric $CO_2$ values are lower in the NH polar region than those at midlatitudes during this season, which is partly related to the transport of stratospheric low-$CO_2$ air into the midtroposphere over the NH polar region [*Jiang et al.*, 2013b].

In April (Figure 1b), the latitudinal gradients of $CO_2$ have the same sign among GOSAT $X_{CO2}$, AIRS midtropospheric $CO_2$, TES midtropospheric $CO_2$, TCCON $X_{CO2}$, and NOAA-ESRL surface $CO_2$. There is more $CO_2$ in the NH high latitudes in April as a result of building up of fossil fuel emissions and biomass burning in the winter season. The NOAA-ESRL surface $CO_2$ measurements are higher than those from GOSAT $X_{CO2}$ and the AIRS and TES midtropospheric $CO_2$ in the NH. The concentration of $CO_2$ is low at NH high latitudes in July due to the uptake of $CO_2$ by the biosphere [*Pearman and Hyson*, 1981; *Keeling et al.*, 1996, see Figure 1c]. The $CO_2$ concentrations are lower in the surface NOAA-ESRL $CO_2$ than those in the satellite $CO_2$ retrievals (GOSAT $X_{CO2}$, TCCON $X_{CO2}$, and AIRS midtropospheric $CO_2$) in the NH in July. $CO_2$ concentrations increase again in the NH high latitudes in October [*Keeling et al.*, 1996; *Giglio et al.*, 2006; *Randerson et al.*, 2013] as shown in Figure 1d. The differences among the three satellite $CO_2$ retrievals are related to the different vertical sensitivities of the three satellite $CO_2$ observations.

In Figure 2, we compared zonal mean $CO_2$ time series from three satellite $CO_2$ retrievals and the NOAA-ESRL surface $CO_2$. $CO_2$ annual cycle amplitudes are larger in the NH than that in the SH, because the amplitudes of the $CO_2$ annual cycles from biospheric photosynthesis and respiration are larger in the NH than that in the SH [*Cleveland et al.*, 1983]. $CO_2$ seasonal cycle amplitudes also change as a function of time as shown in Figure 2. To better reveal $CO_2$ annual cycle amplitudes as a function of latitude, we have applied a multiple regression method to all data sets. We regressed $CO_2$ data to the trend, annual, and semiannual oscillation. We decomposed $CO_2$ concentrations, $X$, at each location using the following empirical model [*Jiang et al.*, 2013a]:

$$\begin{aligned} X(t) = A_0 + A_1 N P_1(t/N-1) + A_2 N^2 P_2(t/N-1) + A_3 N^3 P_3(t/N-1) \\ + C_1\cos(2\pi t) + S_1\sin(2\pi t) + C_2\cos(4\pi t) + S_2\sin(4\pi t) \end{aligned} \quad (1)$$

where $t$ is time, $N$ is the half length of the time period, the values $P_1$, $P_2$, and $P_3$ are the first, second, and third Legendre polynomials. The coefficients $A_0$, $A_1$, $A_2$, and $A_3$ are the mean value, the trend, the acceleration in the trend, and the coefficient for $P_3$, respectively. We added the third Legendre function to better fit the data sets. Annual and semiannual cycles are represented by the harmonic functions. $C_1$ and $S_1$ are the amplitudes of the annual cycle, while $C_2$ and $S_2$ are the amplitudes of the semiannual cycle.

The amplitudes for the $CO_2$ annual cycle ($\sqrt{C_1^2+S_1^2}$) and the $CO_2$ semiannual cycle ($\sqrt{C_2^2+S_2^2}$) are plotted in Figures 3a and 3b, respectively. The $CO_2$ annual cycle amplitudes are ~5–10 ppm for the NOAA-ESRL surface $CO_2$ in the NH, which is almost a factor of 2 larger than those derived from the satellite $CO_2$ retrievals. The annual cycle amplitudes of the GOSAT $X_{CO2}$ are consistent with those from TCCON $X_{CO2}$. For these two

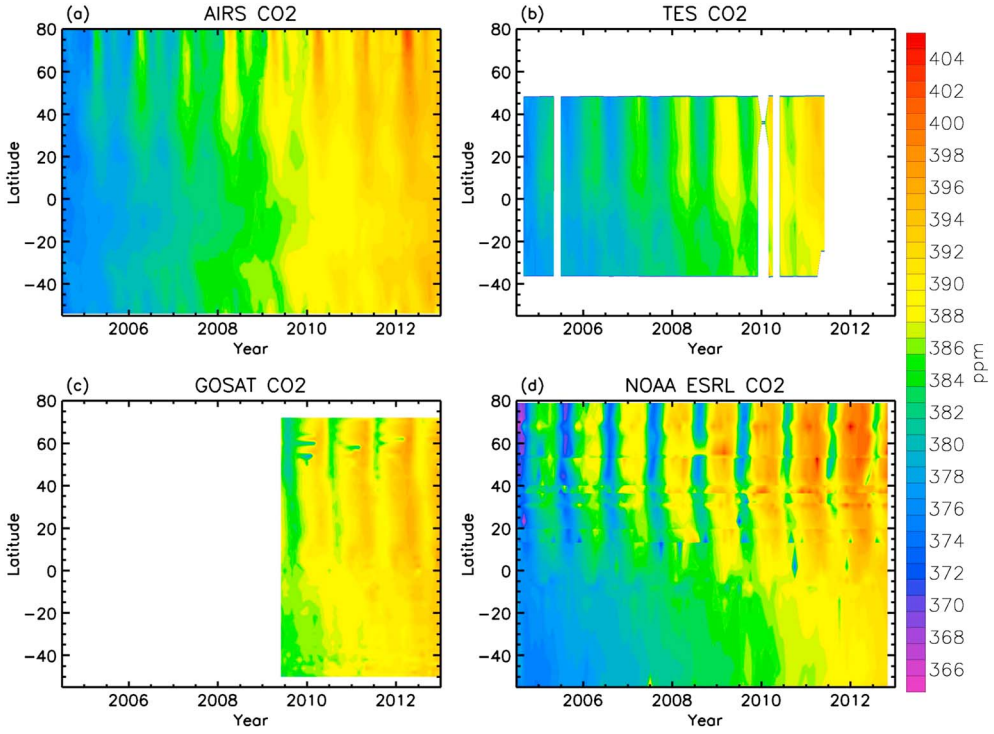


**Figure 2.** (a) Zonal mean AIRS midtropospheric $CO_2$, (b) zonal mean TES midtropospheric $CO_2$, (c) zonal mean GOSAT $X_{CO2}$, and (d) surface NOAA-ESRL $CO_2$.

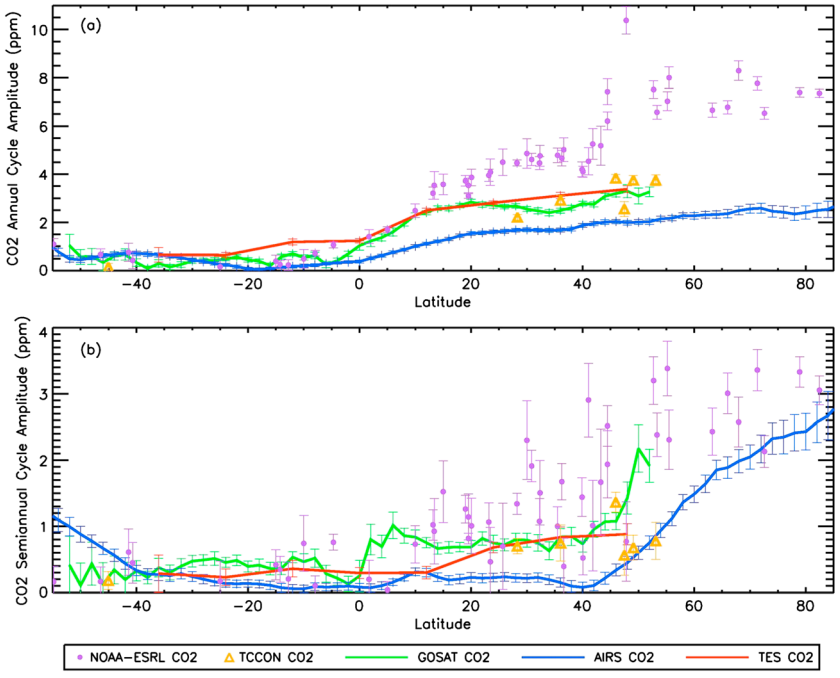


**Figure 3.** (a) Latitudinal distributions of $CO_2$ annual cycle amplitudes. (b) Latitudinal distributions of $CO_2$ semiannual cycle amplitudes. Blue lines are results from AIRS midtropospheric $CO_2$. Green lines are results from GOSAT $X_{CO2}$. Purple dots are results from NOAA-ESRL surface $CO_2$. Orange triangles are results from TCCON $X_{CO2}$. Error bars are the uncertainties of $CO_2$ annual cycle and semiannual cycle amplitudes derived from the multiple regressions.

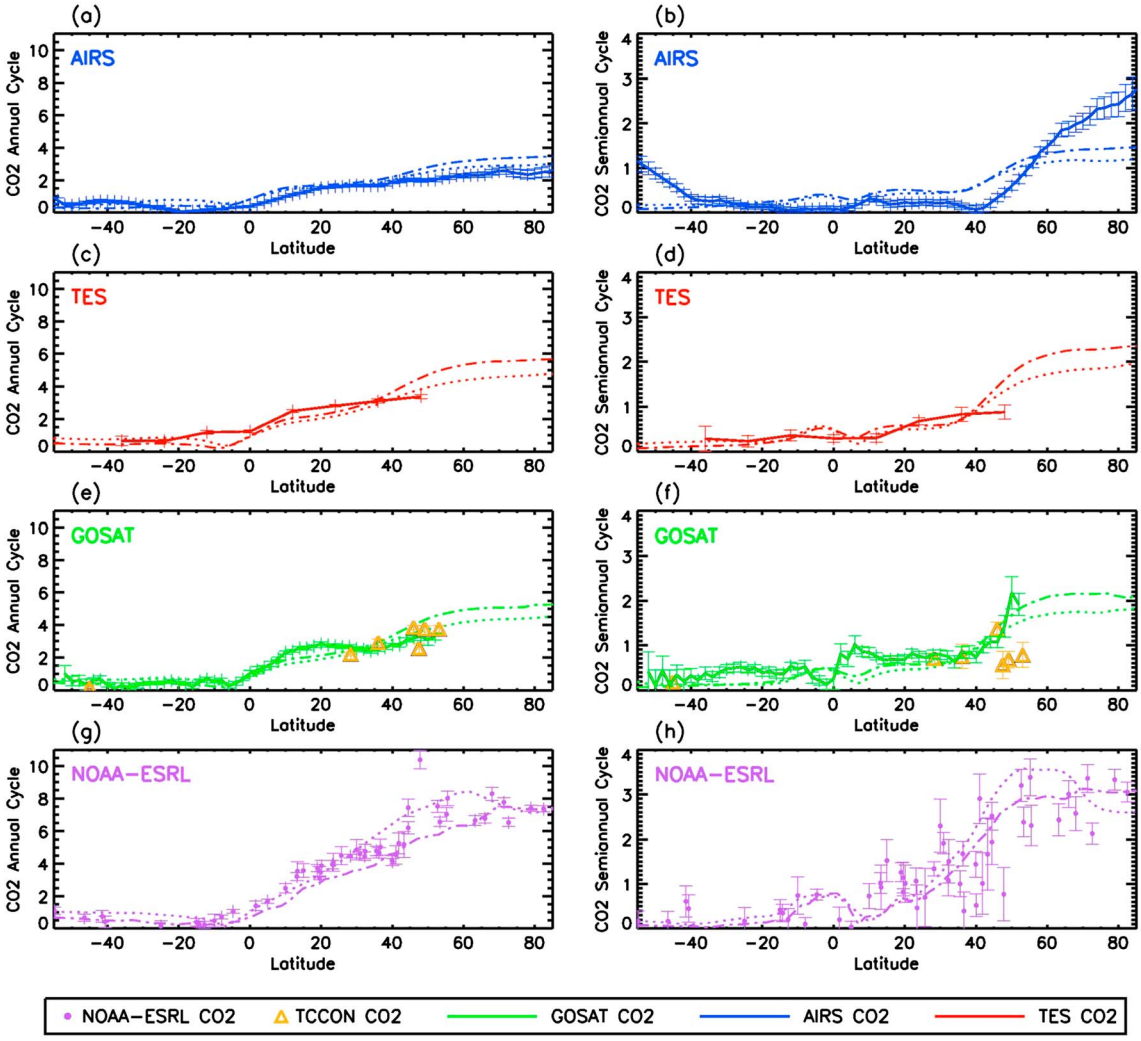


**Figure 4.** (a) Comparison of annual cycle amplitudes between AIRS midtropospheric $CO_2$ and model convolved $CO_2$, (b) comparison of semiannual cycle amplitudes between AIRS midtropospheric $CO_2$ and model convolved $CO_2$, (c and d) comparisons of annual and semiannual cycle amplitudes between TES midtropospheric $CO_2$ and model convolved $CO_2$, (e and f) comparisons of annual and semiannual cycle amplitudes between GOSAT $X_{CO2}$ and model convolved $CO_2$, and (g and h) comparisons of annual and semiannual cycle amplitudes between NOAA-ESRL surface $CO_2$ and model surface $CO_2$. Dotted lines are convolved model $CO_2$ from MOZART-2. Dash-dotted lines are convolved model $CO_2$ from CarbonTracker. Units are in ppm.

$X_{CO2}$ data sets, the NH (SH) annual cycle amplitudes are about 2–3 ppm (0.5–1 ppm). TES $CO_2$ annual cycle amplitudes are similar to GOSAT $X_{CO2}$ in the NH. The NH $CO_2$ annual cycle amplitude is smallest in the AIRS midtropospheric $CO_2$. Since the $CO_2$ annual cycle amplitudes are small in the SH, the differences of $CO_2$ annual cycle amplitudes between different satellite $CO_2$ retrievals are correspondingly small.

Amplitudes for $CO_2$ semiannual cycle are shown in Figure 3b. The $CO_2$ semiannual signal is largest at the surface, for the source for the semiannual signal in $CO_2$ is mostly related to the $CO_2$ exchange between biosphere and atmosphere at the surface [*Jiang et al.*, 2012]. The $CO_2$ semiannual signals are consistent between the GOSAT and TCCON $CO_2$, which are smaller than that from the surface NOAA-ESRL $CO_2$. The semiannual signal is smaller in the AIRS midtropospheric $CO_2$ than GOSAT $CO_2$ and TES $CO_2$.

Similar multiple regression analysis has been applied to model $CO_2$ from MOZART-2 and CarbonTracker to check how well the models simulate the annual and semiannual cycles of $CO_2$ at different altitudes. First, we convolve GOSAT, TES, and AIRS averaging kernels with the MOZART-2 and CarbonTracker model vertical $CO_2$ profiles. Then we calculate the $CO_2$ annual cycle amplitude ($\sqrt{C_1^2 + S_1^2}$) and semiannual cycle amplitude ($\sqrt{C_2^2 + S_2^2}$) for model convolved $CO_2$ using the multiple regression method. Results for the annual cycle

and semiannual cycle amplitudes from the model convolved $CO_2$ are plotted against satellite and surface $CO_2$ in Figure 4. The convolved model $CO_2$ annual cycle amplitudes are shown in Figures 4a, 4c, 4e, and 4g. In the midlatitudes of the NH, the model convolved $CO_2$ annual cycle amplitudes are about 2–3 ppm, which are a little (~0.5 ppm) lower than the amplitudes seen in the satellite $CO_2$ retrievals from GOSAT and TES. In the midlatitudes of the NH, the model surface $CO_2$ annual cycle amplitudes are similar to those obtained from the NOAA-ESRL surface $CO_2$. The model convolved $CO_2$ annual cycle amplitude (blue line) is about 3 ppm in the NH high latitudes, which is close to that in the AIRS midtropospheric $CO_2$ as shown in Figure 4a. In the SH, the model results convolved with the remote sensing averaging kernels produce $CO_2$ annual cycle amplitudes between 0.5 and 1 ppm, which are similar to those from GOSAT, TES, and AIRS $CO_2$ retrievals. The values obtained by convolving the model $CO_2$ by the GOSAT averaging kernel are larger than the values obtained by convolving the model $CO_2$ by the AIRS $CO_2$ averaging kernel, because the GOSAT $X_{CO2}$ averaging kernel's maximum is closer to the surface than that for the AIRS $CO_2$ averaging kernel.

Semiannual cycle amplitudes for the MOZART-2 and CarbonTracker $CO_2$ are shown in Figures 4b, 4d, 4f, and 4h. Both models show $CO_2$ semiannual cycles that are larger in the NH than SH. The $CO_2$ semiannual cycle amplitude obtained by convolving the models with the GOSAT averaging kernel is about 0.5–2 ppm in the NH, which is similar to the measured GOSAT $CO_2$ semiannual cycle shown in Figure 4f. The amplitude of the $CO_2$ semiannual cycle obtained by convolving the models with the AIRS averaging kernel is about 0.5–1 ppm in the NH, which is weaker than that from AIRS $CO_2$ semiannual cycle in the high latitudes. In the SH, the amplitudes of the semiannual cycle in $CO_2$ obtained by convolving the model results with the AIRS averaging kernel is much weaker than in the NH, which is consistent with the observation. The difference of the $CO_2$ semiannual cycle amplitudes between AIRS midtropospheric $CO_2$ and model convolved $CO_2$ is ~0.5–1 ppm in the high latitudes and need further exploration with in situ $CO_2$ profile data in the future.

## 4. Conclusions

Recent satellite $CO_2$ retrievals offer a unique opportunity to study the $CO_2$ variability at different altitudes [*Crisp et al.*, 2012; *Chahine et al.*, 2008; *Kulawik et al.*, 2010]. In this paper, we have compared the satellite $CO_2$ retrievals with in situ $CO_2$ measurements (NOAA-ESRL surface $CO_2$ and TCCON $X_{CO2}$). The latitudinal gradients and their seasonal variations are consistent with the vertical sensitivities of the observations and the rapid decay of the $CO_2$ variations with altitude. We have investigated the annual cycle and semiannual cycle amplitudes of $CO_2$ from the GOSAT $X_{CO2}$, midtropospheric AIRS $CO_2$, midtropospheric TES $CO_2$, NOAA-ESRL surface $CO_2$, and TCCON $X_{CO2}$. The $CO_2$ annual cycle and semiannual cycle amplitudes for GOSAT $X_{CO2}$ and TCCON $X_{CO2}$ are consistent but smaller than those seen in the NOAA-ESRL surface data. As expected, the $CO_2$ annual cycle and semiannual cycle amplitudes are larger in the NH than that in the SH. The $CO_2$ annual and semiannual cycles are smallest in the AIRS midtropospheric $CO_2$ compared with other data sets in the NH. The amplitudes for the $CO_2$ annual cycle and semiannual cycle from GOSAT, TES, and AIRS $CO_2$ are small and comparable to each other in the SH. Results obtained in this study can help us better understand the information contents of the satellite $CO_2$ retrievals and vertical structures for the $CO_2$ annual cycle and semiannual cycle. Comparisons of these ground-based and satellite observations with the MOZART-2 and CarbonTracker model illustrate how well the chemistry-transport models simulate the $CO_2$ annual cycles and semiannual cycles at different altitudes. With better $CO_2$ surface emission inventories and transport fields, we can better simulate $CO_2$ seasonal cycles at different altitudes in the future. These data/model comparisons can also be used to diagnose the deficiencies in the models and improve the $CO_2$ simulations, which is very important for understanding the carbon budget in the future.

**Acknowledgments**

We thank M. Gerstell, anonymous reviewers, and the Editor for the helpful comments. CarbonTracker CT 2013 results are provided by NOAA ESRL, Boulder, Colorado, USA from the website at http://carbontracker.noaa.gov/. TCCON results are obtained from the TCCON data archive, operated by the California Institute of Technology from the website at http://tccon.ipac.caltech.edu/. X. Jiang and YLY were supported by NASA grant NNX13AK34G to Caltech and UH. Part of the research was carried out at the Jet Propulsion Laboratory, California Institute of Technology, under a contract with the National Aeronautics and Space Administration.

## References

Aumann, H. H., et al. (2003), AIRS/AMSU/HSB on the Aqua mission: Design, science objectives, data products, and processing systems, *IEEE Trans. Geosci. Remote Sens.*, *41*, 253–264.

Bacastow, R. (1976), Modulation of atmospheric carbon dioxide by the Southern Oscillation, *Nature*, *261*, 116–118.

Bacastow, R. B., C. D. Keeling, and T. P. Whorf (1985), Seasonal amplitude increase in atmospheric $CO_2$ concentration at Mauna Loa, Hawaii, 1959–1982, *J. Geophys. Res.*, *90*, 10,529–10,540, doi:10.1029/JD090iD06p10529.

Bacastow, R., J. Adams, C. D. Keeling, D. Moss, T. Whorf, and C. Wong (1980), Atmospheric carbon dioxide, the Southern Oscillation, and the weak 1975 El Niño, *Science*, *210*, 66–68.

Beer, R. (2006), TES on the Aura mission: Scientific objectives, measurements, and analysis overview, *IEEE T. Geosci. Remote*, *44*, 1102–1105.

Boden, T. A., G. Marland, and R. J. Andres (2013), *Global, Regional, and National Fossil-Fuel $CO_2$ Emissions*, Carbon Dioxide Information Analysis Center, Oak Ridge Natl. Lab., Oak Ridge, Tenn., doi:10.3334/CDIAC/00001_V2013.

Boesch, H., et al. (2006), Space-based near-infrared $CO_2$ measurements: Testing the Orbiting Carbon Observatory retrieval algorithm and validation concept using SCIAMACHY observations over Park Falls, Wisconsin, *J. Geophys. Res.*, *111*, D23302, doi:10.1029/2006JD007080.

Boesch, H., D. Baker, B. Connor, D. Crisp, and C. Miller (2011), Global characterization of $CO_2$ column retrievals from shortwave-infrared satellite observations of the Orbiting Carbon Observatory-2 Mission, *Remote Sens.*, *3*, 270–304.

Bowman, K. W., et al. (2006), Tropospheric emission spectrometer: Retrieval method and error analysis, *IEEE T. Geosci. Remote*, *44*, 1297–1307.

Buermann, W., B. Lintner, C. Koven, A. Angert, J. E. Pinzon, C. J. Tucker, and I. Fung (2007), The changing carbon cycle at the Mauna Loa Observatory, *Proc. Natl. Acad. Sci.*, *104*, 4249–4254.

Chahine, M., C. Barnet, E. T. Olsen, L. Chen, and E. Maddy (2005), On the determination of atmospheric minor gases by the method of vanishing partial derivatives with application to $CO_2$, *Geophys. Res. Lett.*, *32*, L22803, doi:10.1029/2005GL024165.

Chahine, M., L. Chen, P. Dimotakis, X. Jiang, Q. Li, E. T. Olsen, T. Pagano, J. Randerson, and Y. L. Yung (2008), Satellite remote sounding of mid-tropospheric $CO_2$, *Geophys. Res. Lett.*, *35*, L17807, doi:10.1029/2008GL035022.

Cleveland, M. S., A. E. Freeny, and T. E. Graedel (1983), The seasonal component of atmospheric CO2: Information from new approaches to the decomposition of seasonal time series, *J. Geophys. Res.*, *88*, 10,934–10,946, doi:10.1029/JC088iC15p10934.

Connor, B. J., H. Boesch, G. Toon, B. Sen, C. Miller, and D. Crisp (2008), Orbiting Carbon Observatory: Inverse method and prospective error analysis, *J. Geophys. Res.*, *113*, D05305, doi:10.1029/2006JD008336.

Crisp, D., et al. (2012), The ACOS $X_{CO2}$ retrieval algorithm. Part 2: Global $X_{CO2}$ data characterization, *Atmos. Meas. Tech.*, *5*, 687–707.

Dargaville, R. J., R. M. Law, and F. Pribac (2000), Implications of interannual variability in atmospheric circulation on modeled $CO_2$ concentrations and source estimates, *Global Biogeochem. Cycles*, *14*, 931–943, doi:10.1029/1999GB001166.

Dettinger, M. D., and M. Ghil (1998), Seasonal and interannual variations of atmospheric $CO_2$ and climate, *Tellus Ser. B*, *50*, 1–24.

Enting, I. G. (1987), The interannual variation in the seasonal cycle of carbon dioxide concentration at Mauna Loa, *J. Geophys. Res.*, *92*, 5497–5504, doi:10.1029/JD092iD05p05497.

Feely, R. A., et al. (1987), Distribution of chemical tracers in the eastern equatorial Pacific during and after the 1982/1983 ENSO event, *J. Geophys. Res.*, *92*, 6545–6558, doi:10.1029/JC092iC06p06545.

Giglio, L., G. R. van der Werf, J. T. Randerson, G. J. Collatz, and P. S. Kasibhatla (2006), Global estimation of burned area using MODIS active fire observations, *Atmos. Chem. Phys.*, *6*, 957–974.

GLOBALVIEW-CO2 (2010), Cooperative atmospheric data integration project: Carbon dioxide [CD-ROM], *NOAA ESRL Boulder Colorado*. [Available on Internet via anonymous FTP to ftp.cmdl.noaa.gov, Path: ccg/co2/GLOBALVIEW.]

Horowitz, L. W., et al. (2003), A global simulation of tropospheric ozone and related tracers: description and evaluation of MOZART, version 2, *J. Geophys. Res.*, *108*(D24), 4784, doi:10.1029/2002JD002853.

Jacobson, A. R., S. E. M. Fletcher, N. Gruber, J. L. Sarmlento, and M. Gloor (2007), A joint atmosphere–ocean inversion for surface fluxes of carbon dioxide: 2. Regional results, *Global Biogeochem. Cycles*, *21*, GB1020, doi:10.1029/2006GB002703.

Jiang, X., M. T. Chahine, E. T. Olsen, L. Chen, and Y. L. Yung (2010), Interannual variability of mid-tropospheric $CO_2$ from atmospheric infrared sounder, *Geophys. Res. Lett.*, *37*, L13801, doi:10.1029/2010GL042823.

Jiang, X., M. T. Chahine, Q. Li, M. Liang, E. T. Olsen, L. Chen, J. Wang, and Y. L. Yung (2012), $CO_2$ semi-annual oscillation in the middle troposphere and at the surface, *Global Biogeochem. Cycles*, *26*, GB3006, doi:10.1029/2011GB004118.

Jiang, X., J. Wang, E. T. Olsen, M. Liang, T. S. Pagano, L. Chen, S. J. Licata, and Y. L. Yung (2013a), Influence of El Nino on mid-tropospheric $CO_2$ from atmospheric infrared sounder and model, *J. Atmos. Sci.*, *70*, 223–230.

Jiang, X., J. Wang, E. T. Olsen, T. Pagano, L. Chen, and Y. L. Yung (2013b), Influence of stratospheric sudden warming on AIRS mid-tropospheric $CO_2$, *J. Atmos. Sci.*, *70*, 2566–2573.

Jiang, X., E. T. Olsen, T. S. Pagano, H. Su, and Y. L. Yung (2015), Modulation of midtropospheric $CO_2$ by the South Atlantic Walker Circulation, *J. Atmos. Sci.*, *72*, 2241–2247.

Jones, C. D., M. Collins, P. M. Cox, and S. A. Spall (2001), The carbon cycle response to ENSO: A coupled climate-carbon cycle model study, *J. Clim.*, *14*, 4113–4129.

Keeling, C. D., and R. Revelle (1985), Effects of ENSO on the atmospheric content of $CO_2$, *Meteroritics*, *20*, 437–450.

Keeling, C. D., T. P. Whorf, M. Wahlen, and J. Vanderplicht (1995), Interannual extremes in the rate of rise of atmospheric carbon dioxide since 1980, *Nature*, *375*, 666–670.

Keeling, C. D., J. F. S. Chin, and T. P. Whorf (1996), Increased activity of northern hemispheric vegetation inferred from atmospheric $CO_2$ measurements, *Nature*, *382*, 146–149.

Keppel-Aleks, G., P. O. Wennberg, and T. Schneider (2011), Sources of variations in total column carbon dioxide, *Atmos. Chem. Phys.*, *11*, 3581–3593.

Keppel-Aleks, G., et al. (2012), The imprint of surface fluxes and transport on variations in total column carbon dioxide, *Biogeosciences*, *9*, 875–891.

Kulawik, S. S., et al. (2010), Characterization of Tropospheric Emission Spectrometer (TES) $CO_2$ for carbon cycle science, *Atmos. Chem. Phys.*, *10*, 5601–5623.

Kuze, A., H. Suto, M. Nakajima, and T. Hamazaki (2009), Thermal and near infrared sensor for carbon observation Fourier- transform spectrometer on the Greenhouse Gases Observing Satellite for greenhouse gases monitoring, *Appl. Opt.*, *48*, 6716–6733.

Li, K. F., B. Tian, D. E. Waliser, and Y. L. Yung (2010), Tropical mid-tropospheric $CO_2$ variability driven by the Madden-Julian Oscillation, *Proc. Natl. Acad. Sci. U.S.A.*, *107*, 19,171–19,175.

Lin, S. J., and R. B. Rood (1996), Multidimensional flux form semi-Lagrangian transport schemes, *Mon. Weather Rev.*, *124*, 2046–2070.

Macatangay, R., T. Warneke, C. Gerbig, S. Korner, R. Ahmadov, M. Heimann, and J. Notholt (2008), A framework for comparing remotely sensed and in-situ $CO_2$ concentrations, *Atmos. Chem. Phys.*, *8*, 2555–2568.

Miller, J. B., et al. (2012), Linking emissions of fossil fuel $CO_2$ and other anthropogenic trace gases using atmospheric $^{14}CO_2$, *J. Geophys. Res.*, *117*, D08302, doi:10.1029/2011JD017048.

Nevison, C. D., et al. (2008), Contribution of ocean, fossil fuel, land biosphere, and biomass burning carbon fluxes to seasonal and interannual variability in atmospheric $CO_2$, *J. Geophys. Res.*, *113*, G01010, doi:10.1029/2007JG000408.

Nguyen, H., et al. (2014), A method for collocating satellite $X_{CO2}$ data to ground-based data and its application to ACOS-GOSAT and TCCON, *Atmos. Meas. Tech.*, *7*, 2631–2644.

O'Dell, C. W., et al. (2012), The ACOS $CO_2$ retrieval algorithm—Part 1: Description and validation against synthetic observations, *Atmos. Meas. Tech.*, *5*, 99–121.

Oda, T., and S. Maksyutov (2011), A very high-resolution (1km x 1km) global fossil fuel $CO_2$ emission inventory derived using a point source database and satellite observations of nighttime lights, *Atmos. Chem. Phys.*, *11*, 543–556.

Olsen, E. T., and S. J. Licata (2015), AIRS version 5 release tropospheric $CO_2$ products, *Jet Propulsion Laboratory*, 38 pp. [Available online at http://disc.sci.gsfc.nasa.gov/AIRS/documentation/v5_docs/AIRS_V5_Release_User_Docs/AIRS-V5-Tropospheric-CO2-Products.pdf].

Olsen, E. T., M. T. Chahine, L. Chen, X. Jiang, T. S. Pagano, and Y. L. Yung (2008), Validation of AIRS retrievals of $CO_2$ via comparison to in-situ measurements, Abstract A32B-04 presented at 2008 AGU Fall Meeting, AGU, San Francisco, Calif., 15-19 Dec.

Olsen, S. C., and J. T. Randerson (2004), Differences between surface and column atmospheric $CO_2$ and implications for carbon cycle research, *J. Geophys. Res.*, *109*, D02301, doi:10.1029/2003JD003968.

Pagano, T. S., et al. (2014), Global variability of midtropospheric carbon dioxide as measured by the Atmospheric Infrared Sounder, *J. Appl. Remote Sens.*, *8*, doi:10.1117/1.JRS.8.084984.

Pearman, G. I., and P. Hyson (1980), Activities of the global biosphere as reflected in atmospheric $CO_2$ records, *J. Geophys. Res.*, *85*, 4457–4467, doi:10.1029/JC085iC08p04457.

Pearman, G. I., and P. Hyson (1981), The annual variation of atmospheric $CO_2$ concentration observed in the Northern Hemisphere, *J. Geophys. Res.*, *86*, 9839–9843, doi:10.1029/JC086iC10p09839.

Peters, W., et al. (2007), An atmospheric perspective on North American carbon dioxide exchange: CarbonTracker, *Proc. Natl. Acad. Sci. U.S.A.*, *104*, 18,925–18,930.

Randerson, J. T., G. R. van der Werf, L. Giglio, G. J. Collatz, and P. S. Kasibhatla (2013), Global Fire Emissions Database, version 3 (GFEDv3.1), Data set available on line (http://daac.ornl.gov/) from Oak Ridge National Laboratory Distributed Active Archive Center Oak Ridge USA, doi:10.3334/ORNLDAAC/1191.

Reuter, M., et al. (2011), Retrieval of atmospheric CO2 with enhanced accuracy and precision from SCIAMACHY: Validation with FTS measurements and comparison with model results, *J. Geophys. Res.*, *116*, D04301, doi:10.1029/2010JD015047.

Sarmiento, J. L., and S. Wofsy (1999), A U. S. Carbon Cycle Science Plan—A report of the Carbon and Climate Working Group, *U. S. Global Change Research Program*.

Shiomi, K., et al. (2008), GOSAT Level 1 processing and in-orbit calibration plan, in *Sensors, Systems, and Next-Generation Satellites XII*, edited by R. Meynart et al., *Proc. SPIE*, 7106, doi:10.1117/12.800278.

Takahashi, T., et al. (1997), Global air-sea flux of $CO_2$: An estimate based on measurements of sea-air $pCO_2$ difference, *Proc. Natl. Acad. Sci. U.S.A.*, *94*, 8929.

Takahashi, T., et al. (2009), Climatological mean and decadal change in surface ocean $pCO_2$, and net sea-air $CO_2$ flux over the global oceans, *Deep Sea Res., Part II*, *56*, 554–577.

Tans, P., and R. Keeling (2014), Trends in atmospheric carbon dioxide. [Available at http://www.esrl.noaa.gov/gmd/ccgg/trends/.]

Tans, P., et al. (Eds.) (1998), Carbon cycle, in *Climate Monitoring and Diagnostics Laboratory No. 24 Summary Report 1996–1997*, edited by D. J. Hoffmann et al., chap. 2, pp. 30–51, NOAA Environ. Res. Lab., Boulder, Colo. [Available at http://www.cmdl.noaa.gov/.]

van der Werf, G. R., et al. (2006), Interannual variability in global biomass burning emissions from 1997 to 2004, *Atmos. Chem. Phys.*, *6*, 3423–3441.

Wang, J., X. Jiang, M. T. Chahine, M. C. Liang, E. T. Olsen, L. Chen, S. Licata, T. Pagano, and Y. L. Yung (2011), The influence of Tropospheric Biennial Oscillation on mid-tropospheric $CO_2$, *Geophys. Res. Lett.*, *38*, L20805, doi:10.1029/2011GL049288.

Washenfelder, R. A., G. C. Toon, J.-F. Blavier, Z. Yang, N. T. Allen, P. O. Wennberg, S. A. Vay, D. M. Matross, and B. C. Daube (2006), Carbon dioxide column abundances at the Wisconsin Tall Tower site, *J. Geophys. Res.*, *111*, D22305, doi:10.1029/2006JD007154.

Watanabe, H., H. Ishihara, K. Hayashi, F. Kawazoe, N. Kikuchi, N. Eguchi, T. Matsunaga, and T. Yokota (2008), Detailed design of the GOSAT DHF at NIES and data acquisition/processing/distribution strategy, in *Sensors, Systems, and Next-Generation Satellites XII*, edited by R. Meynart et al., *Proc. SPIE*, 7106, doi:10.1117/12.801238.

Wunch, D., et al. (2011), A method for evaluating bias in global measurement of $CO_2$ total columns from space, *Atmos. Chem. Phys.*, *11*, 12,317–12,337.

Yokota, T., Y. Yoshida, N. Eguchi, Y. Ota, T. Tanaka, H. Watanabe, and S. Maksyutov (2009), Global concentrations of $CO_2$ and $CH_4$ retrieved from GOSAT: First preliminary results, *SOLA*, *5*, 160–163.